Deep UV resonance Raman detection in a liquid core waveguide for online identification and quantification in column liquid chromatography

Philipp Siegmund, Stefan Klinken-Uth, Michael C. Hacker, Jörg Breitkreutz, Björn Fischer

Microchemical Journal 221 (2026) 117063

Contents lists available at ScienceDirect

Microchemical Journal

journal homepage: www.elsevier.com/locate/microc

Deep UV resonance Raman detection in a liquid core waveguide for online identification and quantification in column liquid chromatography

Philipp Siegmund [1], Stefan Klinken-Uth [2], Michael C. Hacker [3], Jörg Breitkreutz [4], Björn Fischer [*,5]

Institute of Pharmaceutics and Biopharmaceutics, Faculty of Mathematics and Natural Sciences, Heinrich Heine University, Universitätsstraße 1, 40225 Düsseldorf, Germany

ARTICLE INFO

Keywords:
Resonance Raman spectroscopy
Liquid chromatography
Liquid-core waveguide
Deep UV laser
Naproxen
Metformin

ABSTRACT

This study presents a novel experimental setup that couples high-performance liquid chromatography (HPLC) with a custom-built deep ultraviolet resonance Raman spectrometer (DUV-RRS) for the identification and quantification of analytes following chromatographic separation. For the first time, a liquid-core waveguide (LCW) was integrated into an HPLC-DUV-RRS system to enhance Raman signal intensity. A cost-efficient and eco-friendly deep UV pulsed laser was employed to achieve this advancement with an average output power of only 0.5 mW. The combination of LCW and DUV-RRS enables strong absorption of the excitation light by the target molecules due to the extended optical pathlength within the LCW. The system's performance was evaluated using two pharmaceutical agents, metformin and naproxen. The detector's sensitivity was found to be compound-dependent. For metformin and naproxen, detection limits of 0.07 µg and 0.20 µg, respectively, were achieved on-column, representing a 3.5-fold and 1.2-fold improvement over previous setups without LCW integration, even though the exposure time of the Raman detector was reduced by a factor of up to 60. While metformin showed a linear correlation between Raman signal intensity and concentration at lower concentrations, no linear relationship could be observed for naproxen due to absorption effects. Nevertheless, partial least squares (PLS) analysis revealed a linear relationship between signal intensity and analyte concentration for both substances across the full tested concentration range. These findings demonstrate the potential of LCW-enhanced DUV-RRS as a sensitive and selective detection method in hyphenated analytical systems, particularly for analytes with favorable resonance Raman properties.

1. Introduction

The combination of liquid chromatography (LC) with various detectors has become the standard analytical approach over recent decades for identifying and testing the purity of chemicals, particularly active pharmaceutical ingredients (API). Both, the LC technique and the detectors have continuously evolved to improve analytical performance. In the scientific literature and practice, the described detectors include UV/VIS spectroscopy, fluorescence detection, mass spectrometry (MS), evaporative light scattering detection, charged aerosol detection, refractive index detection, nuclear magnetic resonance spectroscopy (NMR) and Raman spectroscopy, including deep UV resonance Raman spectroscopy, as well as various combinations of these methods. While MS remains a widely used tool, there is a lack of structural elucidation detectors beyond MS. Techniques such as NMR and Raman spectroscopy offer promising solutions to fill this gap, driving ongoing development efforts in this area [1–5].

A modern detector for structural elucidation is expected to be user-

* Corresponding author.
E-mail addresses: philipp.siegmund@hhu.de (P. Siegmund), stefan.klinken-uth@hhu.de (S. Klinken-Uth), michael.hacker@hhu.de (M.C. Hacker), joerg.breitkreutz@hhu.de (J. Breitkreutz), bjoern.fischer@hhu.de (B. Fischer).
[1] Orcid: 0009-0001–9567-6112.
[2] Orcid: 0009–0008–7060-8552.
[3] Orcid: 0000–0002–4776-2294.
[4] Orcid: 0000-0002-3982-9823.
[5] Orcid: 0000-0002-2868-8754.

https://doi.org/10.1016/j.microc.2026.117063
Received 26 August 2025; Received in revised form 19 January 2026; Accepted 20 January 2026
Available online 21 January 2026

friendly, resource-efficient, environmentally sustainable and cost-effective. These are key characteristics increasingly anticipated in newly developed systems to ensure broad applicability in routine and advanced analytical settings. Among the various detectors, the LC-UV/VIS combination has met many of these criteria and is widely used due to its cost-effectiveness and broad applicability for quantification and identification [6–8]. The substance-specific retention time provided by chromatographic separation, coupled with the high sensitivity of UV/VIS detection, has proven consistently effective. Over time improvements in column technology, methodologies and system parameters have been progressively optimized. In this manner, the resolution of the chromatograms was enhanced, the method time was reduced and the amount of mobile phase consumed was decreased, thereby increasing environmental friendliness.

One limitation of this type of analysis remains the relatively nonspecific character of UV/VIS spectra, which has not been overcome yet. Structural isomers and structurally nearly identical molecules are difficult to distinguish [9]. They often exhibit very similar UV absorption spectra and nearly identical retention times. To challenge the role of UV/VIS detection in analytical chemistry, a newly developed detector must overcome current limitations. Mass spectroscopy holds great potential in this regard. However, this method is complex, expensive, and requires extensive maintenance. Furthermore, it is necessary to have highly trained personnel to operate it effectively. Additionally, it is a destructive technique, which prevents the further use of the analytes [7,10]. To address these limitations, the integration of Raman spectroscopy with UV/VIS offers complementary information, enhancing molecular analysis. While Raman is unlikely to replace UV/VIS as the primary detection method, its combined use provides additional structural insights, leading to a more comprehensive method for quantification and identification.

Raman spectroscopy is a valuable tool for molecule identification and quantification [11,12]. However, in comparison to other spectroscopic techniques like UV/VIS or mass spectrometry, its sensitivity is rather poor [13]. Enhancements in Raman sensitivity have been achieved with various approaches, including surface-enhanced Raman spectroscopy, confocal Raman microscopy, liquid core waveguides (LCW), and resonance Raman spectroscopy (RRS) [4,14]. In RRS, the excitation wavelength must be close to an electronic absorption band of the molecule. Only the vibrations linked to the chromophore group are enhanced in the spectrum [4].

The enhancement of these specific bands in the spectrum ranges by a factor of 10^2 to 10^6 [15]. Since many molecules absorb in the UV range, UV-RRS as a specific form of RRS, holds the potential to increase the Raman signal of a wide range of molecules [16–18]. Another advantage is the suppression of interfering fluorescence, achieved by utilizing an excitation wavelength in the deep UV region [19]. Liquid-core waveguides amplify the measurement signal by increasing the sample volume that interacts with the excitation light source [20]. It was demonstrated that LCW's in the visible range can enhance the signal intensity of Raman signals up to a factor of 1000 [21].

The aim of this study is to develop a highly sensitive Raman detector by combining deep UV resonance excitation with a liquid-core waveguide to overcome the low sensitivity of Raman scattering, which remains a major obstacle for the practical implementation of HPLC-coupled Raman detection. In the field of non-resonant Raman spectroscopy, couplings with an LCW for LC applications have already been demonstrated [5,21,22]. More recently, size-exclusion chromatography (SEC) has been coupled with a Raman detector employing an LCW for biomarker, biopharmaceutical, and protein analysis, indicating growing interest in the application of Raman detection in chromatographic systems [23,24]. These approaches, however, were limited to the visible or near-infrared spectral regions and did not involve the use of an organic mobile phase. UV-RRS has also been successfully coupled with HPLC, but not when using an LCW [2,15]. However, a first attempt to combine UV-RRS with an LCW was only successfully carried out using a purely aqueous flow injection [25]. To date, no study has demonstrated such a coupling after an HPLC separation using an organic mobile phase. The detector is to be integrated into an existing LC-UV/VIS system in order to add structural information to the analysis. Due to the strong absorption of the excitation light source by the analyte in the extended path of the LCW, the dominant Raman signal of the organic component in the mobile phase in particular is strongly attenuated during the measurement. In addition, the generated Raman signals from the analyte and mobile phase must also leave the optical waveguide again and can be reabsorbed by the analyte on the path length. This leads to a complex behavior of signal to background signal, which makes an evaluation much more difficult.

The purpose of this study is to advance research in the field of Raman-HPLC coupling by demonstrating for the first time the combination of UV-RRS and LCW in the presence of an organic mobile phase. To evaluate feasibility under realistic chromatographic conditions, metformin and naproxen were selected as pharmaceutical model analytes. The analytes were analyzed online with the Raman detector positioned downstream of the UV/VIS detector after chromatographic separation. In addition to identification based on structural Raman information, the study also uses Partial Least Squares (PLS) analysis to enable quantification with the Raman detector. The PLS model utilizes all spectral changes, including the Raman signal of the analyte, the Raman signals of the solvent and, most importantly, the absorption of all signals by the analyte itself. The analysis of these combined spectral effects should enable identification and quantification with the developed Raman detector.

2. Experimental section

2.1. Chemicals and preparation of samples and mobile phase

High-purity chemicals and reagents were used without further purification. Naproxen sodium (98%) was used as received (BLD Pharmatech GmbH, Kaiserslautern, Germany). Metformin hydrochloride (99.6%) was employed as obtained (Auro Laboratories Limited, Mumbai, India). The used sodium dihydrogen phosphate monohydrate ($\geq$ 99%) was of analytical grade (AppliChem GmbH, Darmstadt, Germany). Water of HPLC Gradient grade was used (Fisher Scientific, Geel, Belgium). Acetonitrile ($\geq$ 99,9%) and methanol (100%) were used as received (VWR Chemicals, Langenfeld, Germany). The listed solvents were utilized for preparing the sample solutions and the mobile phase including the phosphate buffer. For pH adjustment of the phosphate buffer, phosphoric acid 85% (SIGMA-ALDRICH CHEMIE GmbH, Steinheim, Germany) and 1 M sodium hydroxide (Fisher Scientific, Geel, Belgium) were used.

2.2. HPLC system

The configuration of the HPLC system (Dionex, Sunnyvale, California, USA) used in this study is shown in Table 1.

2.3. Deep UV resonance Raman detector with liquid-core waveguide

The experimental setup of the Deep UV Resonance Raman Detector with Liquid-Core Waveguide (UV-RRD-LCW) can be seen in Fig. 1. The detector was connected directly to the UV/VIS detector outlet of the

Table 1
Main modules of the Dionex HPLC system.

Device	Model No.
Pump	P 580 A
Autosampler	ASI-100
Column oven	STH 585
UV/VIS Detector	UVD 340 U

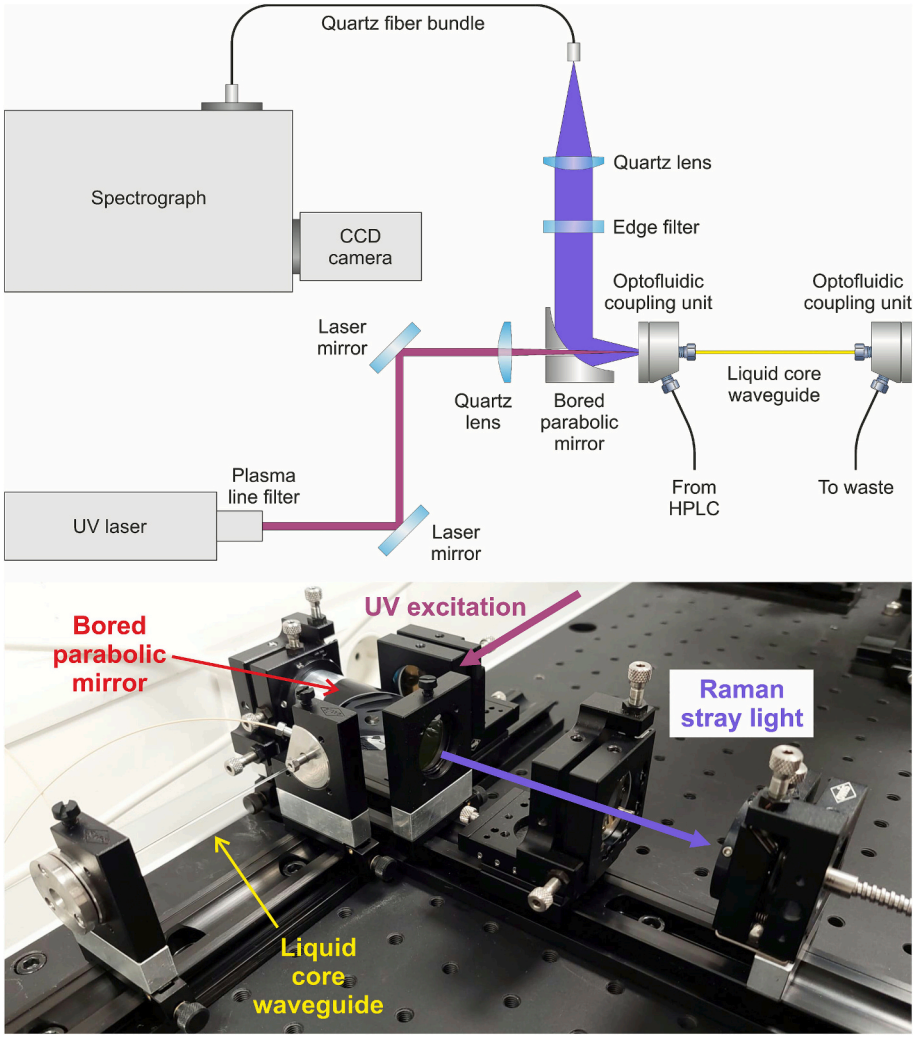

Fig. 1. Experimental setup of the Deep UV Resonance Raman Detector with Liquid-Core Waveguide (UV-RRD-LCW).

HPLC, so that the combined information from UV/VIS and Raman spectroscopy could be used to identify and quantify the substances eluted from the HPLC column. In the UV-RRD-LCW setup, a NeCu 70-248SL excimer laser (Photon Systems Inc., Covina, California, USA) served as the excitation source. This hollow-cathode laser operated at 248.6 nm with a pulse energy of 25 μJ per pulse and a repetition rate of 20 Hz, resulting in an average calculated power of 0.5 mW. All laser parameters were controlled using the DUV Laser.Ink software (Photon Systems Inc., Covina, California, USA).

The measuring cell was constructed using an LCW made from a Teflon AF 2400 capillary with a length of 60 mm (Biogeneral Inc., San Diego, California, USA). The inner diameter of the capillary was 200 μm, resulting in an internal volume of 1.9 μL. In order to seal the flow cell, a fluorinated ethylene propylene (FEP) film was utilized. To allow the laser to pass through this seal unimpeded, a central borehole was introduced as in the work of Kottke et al. described [26]. The laser light was focused into the LCW utilizing two excimer laser mirrors (47–985, Edmund Optics, Barrington, New Jersey, USA) and a quartz lens (LA4647-UV-ML, Thorlabs, Newton, New Jersey, USA). Guided through a bore in a parabolic mirror (11–768, Edmund Optics, Barrington, New Jersey, USA), the laser light was collected by the same mirror after being backscattered, then redirected at a 90° angle while simultaneously being parallelized.

The laser beam, together with Rayleigh scattering was attenuated by means of a long-pass filter (LP02-248RS-25, IDEX Health & Science, LLC, Rochester, New York, USA). The transmitted Raman light was guided to the spectrometer for spectral acquisition. This was achieved by focusing the scattered light into a round-to-linear multimode fiber bundle (BFL105HS02, Ø 105 μm core, Thorlabs, Newton, New Jersey, USA), using a plano-convex quartz lens (LA4148-UV, Thorlabs, Newton, New Jersey, USA). Spectral dispersion was accomplished with a Kymera 328i-B2 spectrometer (Andor Technology / Oxford Instruments plc, Abingdon, UK) equipped with a 2400 lines mm^{-1} diffraction grating optimized for the UV region and providing enhanced efficiency at 300 nm. Detection of the Raman signal was performed with an iDus DV420A-BU2 charge-coupled device camera (Andor Technology / Oxford Instruments plc, Abingdon, UK). Optical alignment and beam positioning were realized using components from the SYS40 series (OWIS GmbH, Staufen, Germany).

2.4. Method development for structural elucidation

The HPLC configurations and operating parameters are presented in Table 2. The methods were developed in close alignment to the European Pharmacopoeia. The composition of the mobile phase varied depending on the analyte.

2.5. Sample preparation

The analytes metformin and naproxen were prepared at the

Table 2
Operating parameters and configurations of the chromatographic setup used for UV resonance Raman analysis of metformin hydrochloride and naproxen sodium.

	Metformin hydrochloride	Naproxen sodium
Column	Zorbax SB-C18 4.6 × 150 mm, 5 µm (Agilent Technologies)	
Mobile phase	A: Phosphate buffer, 10 mM, pH 3 (50%), B: Methanol (50%)	A: Phosphate buffer, 10 mM, pH 3 (30%), B: Acetonitrile (70%)
Run time	5 min	6 min
Temperature	25 °C	
Flow rate	0.5 mL min^{-1}	
Injection volume	20 µL	
UV detection	250 nm	

concentrations specified in Table 3 for the measurements. All samples were prepared in the respective mobile phase of the LC method outlined above. Additionally, a blank solution was prepared from each of the mentioned mobile phases.

2.6. Acquisition of deep UV resonance Raman spectra

Spectrograph measurements were adjusted using the Andor SOLIS 64-bit software. Subsequently, for data analysis, we utilized Origin 2021b (OriginLab Corporation, Northampton, Massachusetts, USA) in combination with Python 3.10.

To ensure high-quality spectra during the chromatographic run, the exposure time was carefully optimized to achieve sufficient signal intensity while minimizing noise. Naproxen required a longer exposure time due to stronger signal interference from the mobile phase compared to metformin. Raman spectra were recorded with an exposure time of 2 s per spectrum for naproxen and 1 s for metformin.

Since the laser could not maintain a stable energy output over extended periods, spectrum acquisition was triggered at the moment the chromatographic peak entered the UV detector located upstream of the Raman unit. During prolonged operation at 20 Hz, the laser exhibited a gradual decrease in pulse energy, which partially recovered when the repetition rate was reduced. This behavior is characteristic of hollow-cathode Ne—Cu UV lasers and has been attributed to thermal and gas-mixture related drift under sustained high-frequency excitation [27]. The observed instability is therefore considered an intrinsic property of the laser rather than a consequence of the optical configuration. By initiating acquisitions only during peak elution and reducing the repetition rate afterwards, the full chromatographic peak could be recorded while preserving laser stability for subsequent runs.

2.7. Univariate data evaluation and assessment of the signal-to-noise ratio

For univariate data processing, the Raman spectra were visualized and processed using OriginLab software. Initially, each spectrum was cropped to a specific range to simplify further analysis. For metformin, the spectral window was extracted between 867 cm^{-1} and 952 cm^{-1}, thereby isolating the main peak at 921 cm^{-1}. For naproxen, the region was cropped from 1602 cm^{-1} to 1678 cm^{-1}, covering the characteristic peak at 1628 cm^{-1}. After spectral acquisition, baseline distortions were corrected using an asymmetric least squares algorithm (asymmetric factor: 0.001, threshold value: 0.005, smoothing factor: 6, number of iterations: 20). To further enhance spectral quality, a Savitzky-Golay smoothing algorithm was applied with a window size of six data points and a second-order polynomial. The Signal-to-Noise (S/N) ratio was then evaluated to determine the detection limit of the Raman signals that could still be attributed to the investigated compounds. For this purpose, the intensity of the representative Raman band was divided by the standard deviation of a signal-free spectral segment. Depending on the composition of the mobile phase, a region of 25 consecutive data points between 1900 and 2000 cm^{-1} (acetonitrile/water) or 2100–2200 cm^{-1} (methanol/water) was used to define the spectral noise. For the signal intensity, the dominant Raman signals for each analyte (Metformin: 921 cm^{-1}, Naproxen: 1628 cm^{-1}) was cropped and baseline-corrected. To verify robustness and reproducibility, the S/N ratio was assessed in three independent measurements.

2.8. Determination of molar absorption coefficients

The molar absorption coefficients (ε) were determined from UV/VIS absorption spectra recorded using a Spectrophotometer UV-1800 (Shimadzu, Japan). Metformin was dissolved in distilled water and naproxen in ethanol. Measurements were performed in standard 1 cm quartz cuvettes at concentrations of 10, 20, 30, 40, and 50 µg mL^{-1}.

Absorbance values were measured at the excitation wavelength (λ_E = 248.6 nm) and at the respective dominant Raman emission wavelengths (λ_M = 254.4 nm for metformin and λ_N = 259.1 nm for naproxen). Linear regressions of absorbance (A) versus concentration (c) were used to determine ε according to the Beer-Lambert law ($A = \varepsilon\ c\ d$, with d = 1 cm). λ_E denotes the excitation wavelength of the laser used for Raman excitation, and λ_R represents the dominant Raman emission wavelength of each analyte. The data were evaluated using Origin (OriginLab Corporation, USA).

2.9. Multivariate cross-decomposition

Partial least-square (PLS) regression in scikit-learn (1.7.0rc1) was utilized to generate prediction models for both analytes. For the data preprocessing, portions of detector capping in the raw spectra were identified by count values above 4×10^4, which reflects the upper dynamic range of the detector with a maximum count capacity of 2 [16]. The full raw spectra were smoothed along the wavenumber axis using a rolling-mean filter with a window width of five data points, corresponding to 0.49% of the full spectral range comprising 1024 wavelengths. Subsequently, a second filtering step was applicated in the direction of time using a Savitzky-Golay filter in SciPy (1.15.2) of a polynomial order of 1 in a width of 3 spectra. The means in the direction of time of the last 5 spectra of each analytical run were defined as the baseline. For every spectrum in the dataset the respective baseline was subtracted, and regions of detector capping were cutout. After this procedure, 470 wavelengths remained for the metformin spectra and 443 wavelengths for the naproxen spectra. The sum of the spectra in the direction of time was calculated, mean centered and standard normal variate scaled, giving the column X. X was subsequently expanded by the interaction terms of every possible combination of signals to introduce nonlinearity into the model. The concentration was log scaled to the base *e* to avoid negative predictions of the concentration at low ranges. For this reason, each prediction was obtained by exponentiating the model output with base *e*. The optimal number of latent structures for the PLS was calculated using the mean-squared-error as the loss metric in a leave-one-out cross-validation.

Table 3
Prepared sample concentrations and injected sample mass on column of naproxen and metformin using an injection volume of 20 µL.

Concentration/µg mL^{-1}	1	2.5	5	10	15	20	25	50	200
Mass on column/µg	0.02	0.05	0.1	0.2	0.3	0.4	0.5	1.0	4.0

3. Results and discussion

3.1. Univariate data processing of metformin

In Fig. 2, the Raman spectrum of metformin is depicted. Fig. 2 A presents the overview spectrum from 500 to 4000 cm^{-1}, while Fig. 2 B displays the fingerprint range between 500 cm^{-1} and 1800 cm^{-1}. The overview spectrum illustrates all Raman signals, including those from the mobile phase. Raman bands assignable to metformin are indicated by wavenumbers, whereas the signal at 921 cm^{-1} stands out as the most dominant one. Excitation at 248.6 nm primarily excites the biguanide chromophore, as this transition can be attributed to an N—H wagging vibration [28]. The signal at 687 cm^{-1} consistently appears in all measurements and can be identified as a laser plasma line (LPL). This attribution is supported by the presence of a previously identified Cu II emission line at 252.9 nm and the known existence of two strong plasma lines of Cu II at 252.66 nm and 252.93 nm in the gas laser discharge [27,29]. Due to the axial alignment of the laser beam and the backward-directed signal collection, the plasma lines are reflected at the entrance window of the liquid-core waveguide and guided towards the detector unit.

In this study, the examined concentration range of metformin, where Raman signals could be reliably assigned to the analyte, spans from 0.05 µg to 4 µg on the column. At lower masses, the S/N ratio for the signal at 921 cm^{-1} was below the detection limit ($S/N < 3.3$). Fig. 2 C and D illustrate the signal intensity of the dominant metformin signal as a function of the injected mass on column. At low masses between 0.05 µg and 0.4 µg on column, a linear relationship between signal intensity and injected analyte mass is visible. Based on the linear regression, the limit of detection (LOD) for metformin was determined to be 0.07 µg on-column, corresponding to a 3.5-fold improvement compared to previous setups without LCW integration [2]. The signal enhancement provided by LCW enabled direct spectral acquisition during peak passage without prolonging its residence time in the Raman flow cell by reducing the flow rate, thereby shortening the spectral acquisition time by a factor of 60. The limit of quantification (LOQ) was 0.23 µg. At concentrations above 0.4 µg on-column, the signal intensity began to plateau, indicating saturation effects.

Since there is a linear relationship between Raman scattering intensity and analyte concentration, Raman detectors can usually be used

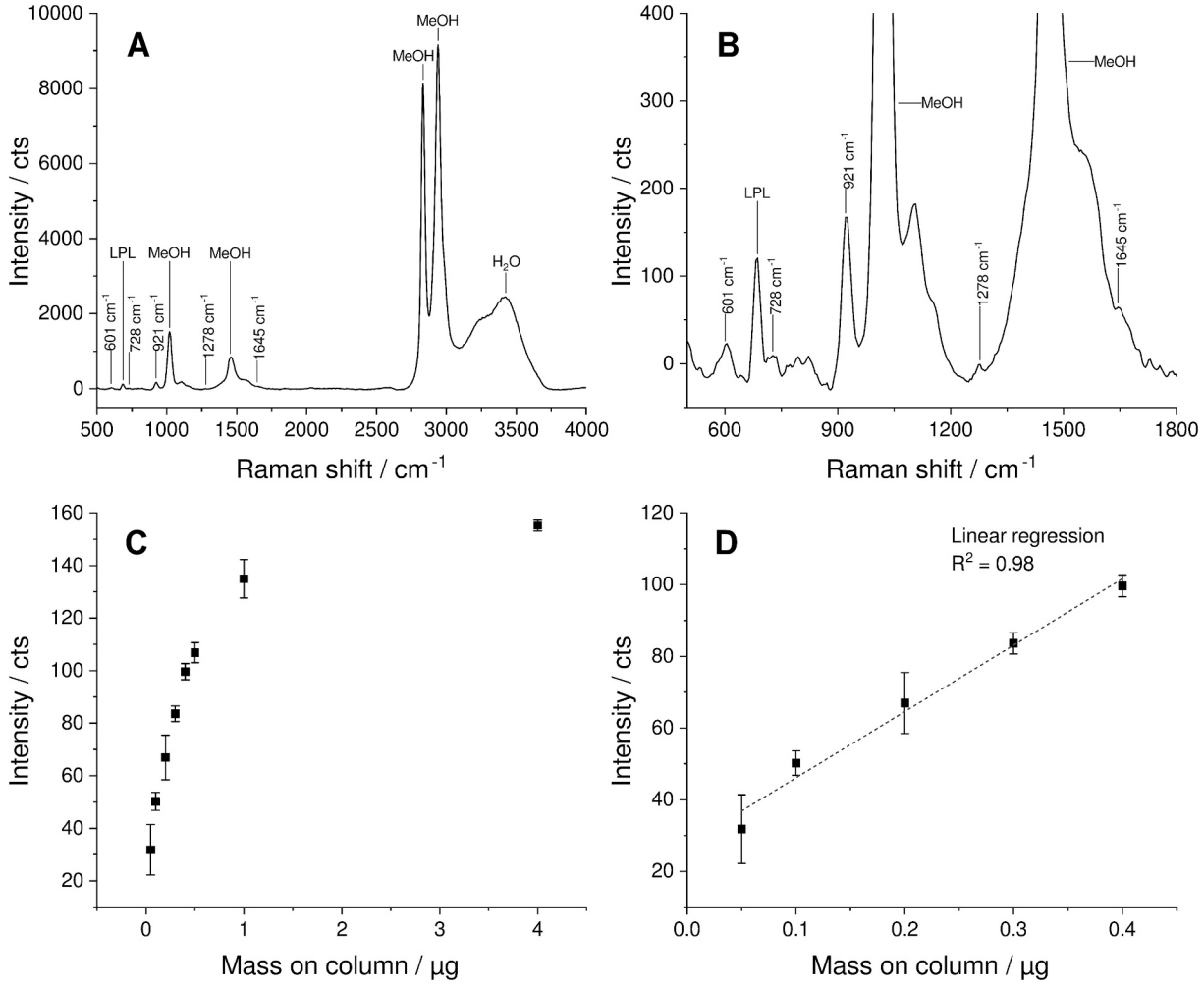

Fig. 2. HPLC-UV-RRD-LCW spectrum of metformin at a concentration of 200 µg mL^{-1} (4 µg on column). Fig. 2 A shows the entire spectral range, highlighting the dominance of solvent bands from methanol (MeOH) and water (H_2O). Fig. 2 B illustrates the Raman fingerprint region of metformin. Raman bands assignable to metformin are indicated by wavenumbers. One peak can be attributed to plasma lines of the laser and is marked as LPL (Laser plasma line). The spectrum consists of averaged spectra with the highest signal-to-noise ratios from the center of the elution peak and was smoothed using the Savitzky-Golay method. Fig. 2 C and D show the signal intensity of the dominant metformin band at 921 cm^{-1} versus the injected mass on column. Fig. 2 C shows the full concentration range (0.05–4 µg on column), where a saturation effect is observed at higher loadings. Fig. 2 D displays the low-concentration subset (0.05–0.4 µg on column), in which a linear relationship is observed, as the saturation effect is not yet present. The saturation at higher loadings is attributed to decreased laser penetration depth in the LCW and increased self-absorption of the analyte's Raman signal.

for quantification as well as substance identification. However, the ability of the detector developed in this study to quantify analytes based on the intensity of their Raman signals is limited as described. A linear relationship between the injected mass on column of the analyte and its Raman signal intensity has already been demonstrated in the deep UV range. In this case the Raman signals were collected from a small focus in a quartz flow cell [2].

A plausible explanation for the limitation of the UV-RRD-LCW is that as the analyte concentration increases, absorption effects reduce the penetration depth of the excitation source in the LCW. Consequently, the excited volume varies depending on the concentration in the LCW. Additionally, self-absorption of the Raman signals contributes to the issue, which in combination affects the linearity of signal intensity in relation to concentration. Both the absorption of the excitation source and the self-absorption of the dominant bands used for quantification are specific to the analyte. Therefore, a linear range cannot be universally defined, as it depends on the substance. In consequence, the Raman signal was detected at the entrance of the LCW in the backward scattering direction, as the excitation light no longer reaches the outlet at higher analyte concentrations and therefore no signal can be detected at the end of the LCW.

3.2. Univariate data processing of naproxen

Fig. 3 A displays the overview spectrum of the second analyte naproxen sodium, Fig. 3 B shows the fingerprint range of naproxen. As mentioned above, the signal of the LPL at 687 cm^{-1} is also visible here. The other marked signals can be attributed to naproxen and the mobile phase. The lower detection limit for the dominant Raman signal at 1628 cm^{-1} was clearly distinguishable from the solvent bands at a mass of 0.2 µg on column. Below this concentration, the S/N fell below the detection limit ($S/N < 3.3$), making reliable detection not possible. This Raman transition can be attributed to the B_3g mode of the ring stretching vibration of naproxen, which appears to be resonantly excited by the laser wavelength at 248.6 nm [30].

With increasing analyte concentration, the Raman signals of the mobile phase decreased. Since the Raman signal of the solvent still lies within the deep UV range, it can be absorbed by the analyte. At the same time, the analyte was resonantly excited, leading to stronger analyte signals, while the non-resonantly excited solvent signals were increasingly suppressed. This effect is due to the stronger interaction of the analyte with the incident laser light compared to the mobile phase. In this context, it is appropriate to discuss the dependence of the linear range on the solvent. If dominant solvent bands overlap with the

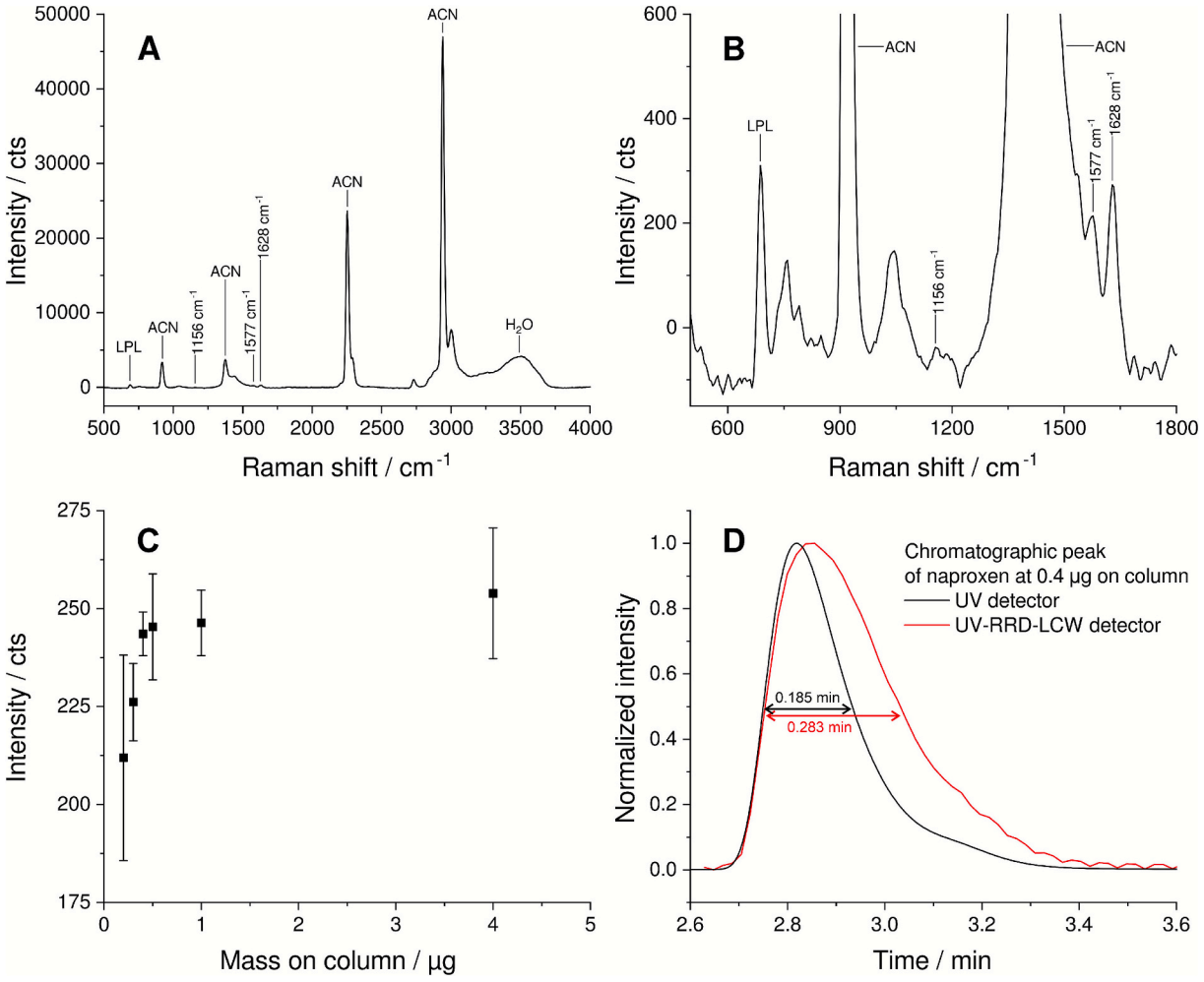

Fig. 3. HPLC-UV-RRD-LCW spectrum of naproxen at a concentration of 200 µg mL^{-1} (4 µg on column). Fig. 3 A shows the entire spectral range, highlighting the dominance of solvent bands from acetonitrile (ACN) and water (H_2O). Fig. 3 B illustrates the Raman fingerprint region of naproxen. Raman bands assignable to naproxen are indicated by wavenumbers. One peak can be attributed to plasma lines of the laser and is marked as LPL (Laser plasma line). The spectrum consists of averaged spectra with the highest signal-to-noise ratios from the center of the elution peak and was smoothed using the Savitzky-Golay method. Fig. 3 C shows the signal intensity of the dominant naproxen band versus injected mass on column. A linear relationship is due to the high standard deviation not depictable. The high standard deviation can be attributed to absorption effects. The first concentration with a S/N of at least 3.3 (limit of detection) in each of the 3 measurements is 0.2 µg on column. Fig. 3 D shows chromatographic peak broadening using the self-built flow cell of the UV-RRD-LCW detector compared to the UV detector of the HPLC.

dominant Raman signal used for quantification, as it is the case for naproxen at 1628 cm^{-1}, the linear range may lie below the detection limit. Unlike metformin, no linear range was observed for naproxen as depicted in Fig. 3 C. The results indicate that the described saturation effect was present nearly throughout the entire concentration range analyzed for naproxen.

Fig. 3 D shows that the self-built UV-RRD-LCW detector causes a broadening of the chromatographic peak compared to the UV detector of the HPLC. To display the elution profile, the total areas under the Raman spectra were integrated and plotted against the time axis. For better comparison, the peak intensities of the two chromatograms were normalized. This shows a peak broadening of the full width at half maximum (FWHM) of 53%, which is due to the design of the flow cell including the LCW.

The two analytes illustrate both the capabilities and limitations of the newly developed detector. While the detector successfully demonstrated its ability to identify both test substances, particularly when combined with LC-UV/VIS, its quantification performance varied depending on the analyte. For metformin, a clear linear range was observed, which allowed for reliable quantification. In contrast, for naproxen, absorption effects prevented the establishment of linearity, making accurate quantification with this detector difficult. These variations arise due to differences in the penetration depth of the excitation source into the liquid-core waveguide (LCW), which is influenced by the properties of the analyte.

3.3. UV absorbance spectra of metformin and naproxen

An explanation for this can be inferred from Fig. 4, which shows the UV absorption spectra of metformin and naproxen. The spectra were recorded via the UV/VIS detector integrated into the developed system. The resonance Raman effect requires at least partial absorption of the excitation wavelength [31,32]. The marked excitation wavelength λ_E indicates the point at which the analytes are excited within the absorption spectrum. Additionally, the entire Raman range up to 4000 cm^{-1} (equivalent to λ_R: 276.1 nm) is shown. The previously described dominant Raman bands of metformin and naproxen are shown in the figure as λ_M and λ_N.

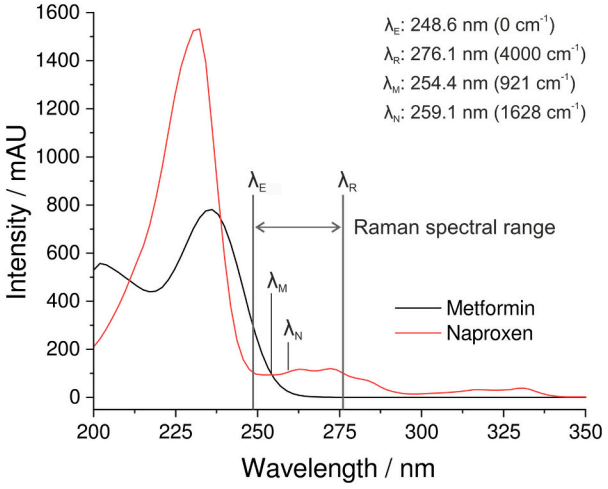

Fig. 4. UV absorption spectra of metformin and naproxen recorded with the UV/VIS detector integrated into the developed system both at a concentration of 50 µg mL^{-1} (1 µg on column). Excitation wavelength λ_E corresponds to the point of analyte excitation within the absorption spectrum. Dominant Raman signals for metformin (λ_M: 254.4 nm) and naproxen (λ_N: 259.1) are highlighted. The entire Raman range up to 4000 cm^{-1} is illustrated (equivalent to λ_R: 276.1 nm). The linear range of metformin is explained by its lower self-absorption ratio compared to naproxen, which is approximately 3 times higher. This results in stronger self-absorption of Raman signals for naproxen.

To explain why a linear range was observed for metformin but not for naproxen, several aspects need to be considered. One possible explanation is the absorption behavior at the excitation wavelength. Fig. 4 shows the UV absorption spectra of metformin and naproxen at a concentration of 50 µg mL^{-1} (1 µg on column). To enable a direct comparison, the raw spectra were overlaid without any normalization or scaling. At this concentration, the absorption of metformin at the excitation wavelength is approximately 300 mAU, while naproxen shows only about 100 mAU. Interestingly, both compounds also show absorption of about 100 mAU at the position of the dominant Raman signals used for quantification.

This raises the question whether the higher absorption of the excitation wavelength alone contributes to the better performance of metformin, or if the ratio between the absorption at the excitation wavelength and the self-absorption at the dominant Raman signal of the analyte is the more decisive factor. This ratio is approximately three times lower for metformin than for naproxen. Accordingly, the Raman signals of naproxen experience stronger overall attenuation due to self-absorption. It is possible that naproxen also exhibits a linear range, but only at lower concentrations, which cannot be detected due to overlapping solvent bands in this experimental setup.

Moreover, the pronounced signal scatter across concentrations observed in Fig. 3 C for naproxen may be related to the fact that the absorption at the excitation wavelength is roughly on the same level as the absorption at the dominant Raman signal itself. This could further limit the reproducibility and quantifiability of the Raman response. Consequently, a higher ratio between absorption at the excitation wavelength and absorption at the Raman emission wavelength results in weaker self-absorption of the analyte bands and therefore supports a more linear relationship between Raman intensity and analyte concentration.

To further quantify the relationship between excitation and emission absorption, the molar absorption coefficients (ε) of both analytes were experimentally determined from UV/VIS absorption spectra recorded over a concentration series. The coefficients were evaluated at the excitation wavelength (λ_E = 248.6 nm) and at the respective dominant Raman emission wavelengths λ_M (metformin) and λ_N (naproxen). The results are summarized in Table 4, which lists the experimentally derived molar absorption coefficients and their ratios.

As shown in Table 4, metformin exhibits a 3.63 times higher absorption at the excitation wavelength compared to its Raman emission region, whereas naproxen absorbs almost equally at both positions. This ratio between excitation and emission absorption increases the probability of self-absorption of the Raman emission in naproxen, which explains the greater deviation from linearity at higher concentrations in the LCW. These quantitative results support the interpretation derived from Fig. 4 and reinforce the discussion on absorption-dependent signal behavior.

3.4. Multivariate data processing

To address the quantification limitations of the univariate processed data, this study proposes a multivariate concentration determination approach. The chosen PLS model primarily utilizes the most significant

Table 4
Molar absorption coefficients (ε) of metformin and naproxen at the excitation λ_E and dominant Raman emission wavelengths $\lambda_{M/N}$, determined from UV/VIS absorption spectra. The table highlights the relationship between excitation and emission absorption.

Analyte	λ_E / nm	$\lambda_{M/N}$ / nm	ε(λ_E) / L mol^{-1} cm^{-1}	ε($\lambda_{M/N}$) / L mol^{-1} cm^{-1}	ε(λ_E) / ε($\lambda_{M/N}$)
Metformin	248.6	254.4	3496.4	964.0	3.63
Naproxen	248.6	259.1	5267.0	5837.1	0.90

changes in the recorded spectra. These changes can be attributed to the increasing absorption of Raman signals associated with the mobile phase as the analyte concentration rises. Furthermore, it also reflects the increasingly intense Raman signals of the analytes themselves.

Due to the capability of PLS regression to model correlation within high dimensional data, the multivariate prediction models for both analytes show promising precision over nearly the full investigated range of concentrations. In the cross-validation of the PLS models, five orthogonal latent components were identified as relevant for predicting the concentration of naproxen, whereas three components were sufficient for metformin. Fig. 5 depicts the calibration plots for both models. It should be noted that the prediction accuracy in the range of the highest concentrations of both APIs is markedly reduced due to the pronounced extremity of these values. To allow a more comprehensive evaluation of the data, the mean relative residuals are plotted in Figs. 5 C and D as a function of the mass on the column. It is clearly evident that the method exhibits deviations of approximately 5% across all concentration levels. Consequently, the precision of the method is, at this stage, not within an acceptable range for reliable quantification. However, it is expected that the precision of the method can be improved by optimizing the laser system and refining the feature selection within the PLS model.

As expected, the chosen multivariate approach was able to identify a linear relationship with respect to concentration. However, at higher concentrations, both substances exhibited pronounced underpredictions of the drug content. Based on this dataset, it cannot be conclusively determined whether these deviations arise from the strong outlier nature of the high-concentration data points or from the inherent limitations of the PLS model in maintaining a linear correlation across the entire concentration range. In this setup, prediction primarily relies on the concentration-dependent attenuation of Raman signals from the mobile phase induced by the analyte. Unlike conventional UV/VIS detection, however, direct absorption of the laser cannot be measured here, as it is blocked by the long-pass filter. Instead, the attenuation of the Raman signals from the mobile phase serves as an indicator of laser attenuation.

4. Conclusion

This study presents a novel Raman detector that for the first time combines HPLC resonance Raman coupling in the deep UV range with a liquid core waveguide. The setup enables Raman spectroscopic analysis of analytes dissolved in an organic mobile phase after HPLC separation. The design represents an improvement in Raman detection and allows measurements at very low concentrations compared to other Raman systems. Metformin was detected at concentrations ranging from 2.5 to 200 µg mL^{-1} (0.05–4.0 µg on the column). For naproxen, the detectable range was observed between 10 and 200 µg mL^{-1} (0.2–4.0 µg on the column). The measurements were conducted using an injection volume of 20 µL and a flow rate of 0.5 mL min^{-1}. These settings are similar to many HPLC methods used, for example, in the European Pharmacopoeia. It is noteworthy, that the results were achieved with an environmentally friendly and resource-saving laser with an average power of approximately 0.5 mW. The univariate data enables the identification of resonantly excited analytes based on substance-specific Raman transitions, especially when combined with the determined retention times by the HPLC and the spectra of the UV/VIS detector. Depending on the analyte, quantification with the Raman detector is possible, but limited by strong absorption effects in the LCW. However, the attenuation of the Raman signals of the mobile phase proved to be useful for multivariate data processing, enabling the establishment of a linear regression. The data from univariate and multivariate data processing can be used in combination for identification and quantification purposes.

Compared to mass spectrometry (MS), the presented detector offers a simple flow cell design similar to UV/VIS detectors and therefore requires less maintenance. In certain applications, it can serve as a cost-effective alternative to MS when sensitivity at low concentrations is not required. Nevertheless, the system should be considered primarily as a complementary detector, especially in combination with UV/VIS, where it provides additional spectroscopic information. However, further optimization of the flow cell is required, particularly of the optofluidic coupling units, in order to counteract excessive peak broadening.

Future studies could also investigate clinically relevant biomarkers as model analytes to further demonstrate the potential of the platform in biomedical and diagnostic contexts. Beyond the present HPLC coupling, the setup could additionally be combined with size exclusion chromatography (SEC) using aqueous phosphate buffers. MS analysis under such conditions is difficult because non-volatile buffers are usually incompatible and buffer exchange is often required. In contrast, the present setup could be operated directly in phosphate-buffered SEC eluents and thus open up perspectives for the investigation of e.g. protein structures. In addition, no significant Raman background of solvent bands is expected in aqueous buffers, which further supports the suitability for protein analysis.

For future work, it would also be beneficial to expand the setup with

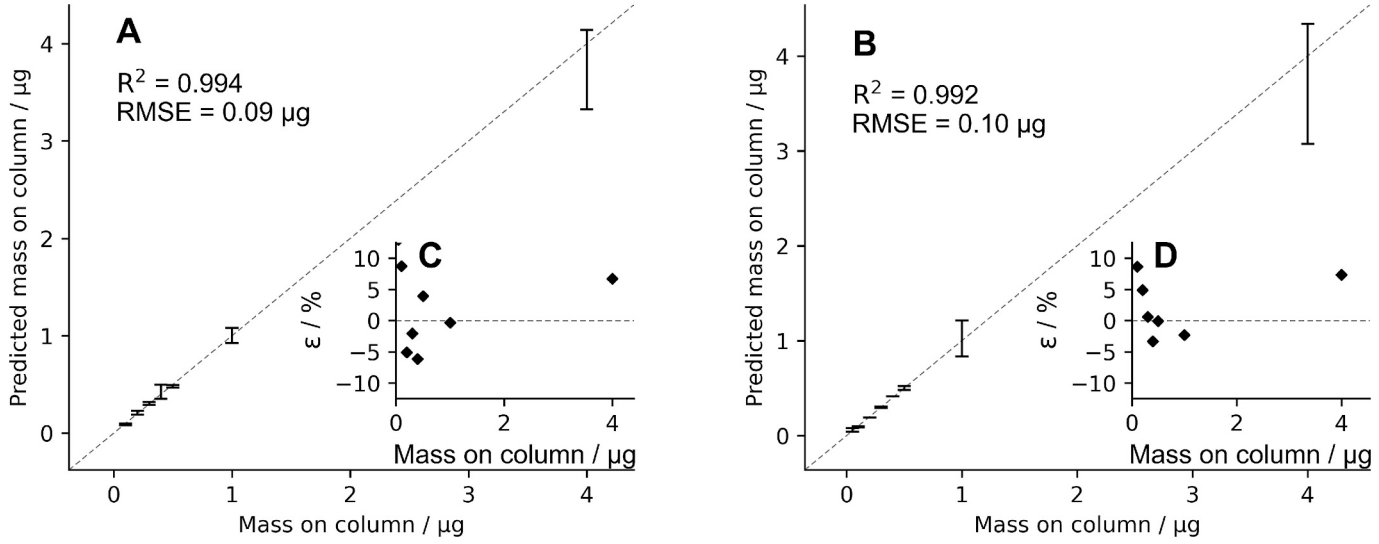

Fig. 5. Calibration plot of cross-validated predictions for naproxen (A) and metformin (B) $\bar{x} \pm s, n = 3$, and means of the relative residuals (C and D).

a tunable UV laser in order to gain deeper insight into the chromophore system with regard to the Raman modes. This could help to determine the best possible ratio between maximum resonant excitation and low reabsorption of Raman scattered light at specific excitation wavelengths, depending on the substance.

Overall, the developed detector shows great potential for the analysis of small molecule drugs in pharmaceutical quality control and at the same time opens a path for future applications in protein analysis. This broader perspective highlights a potential versatility of the demonstrated approach. Systematic studies with an extended range of analytes are required to evaluate its applicability.

CRediT authorship contribution statement

Philipp Siegmund: Writing – original draft, Visualization, Methodology, Investigation, Formal analysis, Data curation, Conceptualization. **Stefan Klinken-Uth:** Writing – review & editing, Writing – original draft, Visualization, Methodology, Formal analysis. **Michael C. Hacker:** Writing – review & editing, Supervision, Conceptualization. **Jörg Breitkreutz:** Writing – review & editing, Supervision, Conceptualization. **Björn Fischer:** Writing – review & editing, Writing – original draft, Visualization, Supervision, Resources, Project administration, Methodology, Funding acquisition, Conceptualization.

Declaration of generative AI and AI-assisted technologies in the writing process

During the preparation of this work the authors used ChatGPT and DeepL in order to improve language and readability. After using these tools, the authors reviewed and edited the content as needed and take full responsibility for the content of the publication.

Declaration of competing interest

The authors declare the following financial interests/personal relationships which may be considered as potential competing interests: Bjoern Fischer reports financial support was provided by Federal Ministry of Economic Affairs and Energy. If there are other authors, they declare that they have no known competing financial interests or personal relationships that could have appeared to influence the work reported in this paper.

Acknowledgements

The authors express their gratitude for the financial support provided by the German Federal Ministry of Economic Affairs and Energy (BMWE) under the agenda for the promotion of Industrial Collective Research (IGF), as approved by the German Bundestag (IGF–Project No. 21280 N).

Data availability

Data will be made available on request.

References

[1] M. Swartz, HPLC detectors: a brief review, J. Liq. Chromatogr. Relat. Technol. 33 (9–12) (2010) 1130–1150, https://doi.org/10.1080/10826076.2010.484356.
[2] P. Siegmund, S. Klinken, M.C. Hacker, J. Breitkreutz, B. Fischer, Application of deep UV resonance Raman spectroscopy to column liquid chromatography: development of a low-flow method for the identification of active pharmaceutical ingredients, Talanta (2024) 126353, https://doi.org/10.1016/j.talanta.2024.126353.
[3] J.C. Lindon, J.K. Nicholson, I.D. Wilson, Directly coupled HPLC–NMR and HPLC–NMR–MS in pharmaceutical research and development, J. Chromatogr. B Biomed. Sci. Appl. 748 (1) (2000) 233–258, https://doi.org/10.1016/S0378-4347(00)00320-0.
[4] E.V. Efremov, F. Ariese, C. Gooijer, Achievements in resonance Raman spectroscopy: review of a technique with a distinct analytical chemistry potential, Anal. Chim. Acta 606 (2) (2008) 119–134, https://doi.org/10.1016/j.aca.2007.11.006.
[5] R.J. Dijkstra, A.N. Bader, G.P. Hoornweg, U.A.T. Brinkman, C. Gooijer, On-line coupling of column liquid chromatography and Raman spectroscopy using a liquid core waveguide, Anal. Chem. 71 (20) (1999) 4575–4579, https://doi.org/10.1021/ac9902648.
[6] Ahuja S, Dong M. Handbook of pharmaceutical analysis by HPLC: Elsevier, 2005. ISBN-13: 978–0080455181.
[7] L. Peltonen, Practical guidelines for the characterization and quality control of pure drug nanoparticles and nano-cocrystals in the pharmaceutical industry, Adv. Drug Deliv. Rev. 131 (2018) 101–115, https://doi.org/10.1016/j.addr.2018.06.009.
[8] S. Marcel, U. Tito, I. Ines, N.J. Pierre, Validation of HPLC-UV method for determination of amoxicillin trihydrate in capsule, Annals Adv. Chem. 2 (2018) 055–072, https://doi.org/10.29328/journal.aac.1001014.
[9] A. Solís-Gómez, R. Sato-Berrú, M. Mata-Zamora, J. Saniger, R. Guirado-López, Characterizing the properties of anticancer silibinin and silybin B complexes with UV–vis, FT-IR, and Raman spectroscopies: a combined experimental and theoretical study, J. Mol. Struct. 1182 (2019) 109–118, https://doi.org/10.1016/j.molstruc.2019.01.042.
[10] A.H. Wu, D. French, Implementation of liquid chromatography/mass spectrometry into the clinical laboratory, Clin. Chim. Acta 420 (2013) 4–10, https://doi.org/10.1016/j.cca.2012.10.026.
[11] G. Fini, Applications of Raman spectroscopy to pharmacy, J. Raman Spectrosc. 35 (5) (2004) 335–337, https://doi.org/10.1002/jrs.1161.
[12] M.J. Pelletier, Quantitative analysis using Raman spectrometry, Appl. Spectrosc. 57 (1) (2003) 20A–42A, https://doi.org/10.1366/000370203321165133.
[13] R. Petry, M. Schmitt, J. Popp, Raman spectroscopy—a prospective tool in the life sciences, chemphyschem 4 (1) (2003) 14–30, https://doi.org/10.1002/cphc.200390004.
[14] R.S. Das, Y. Agrawal, Raman spectroscopy: recent advancements, techniques and applications, Vib. Spectrosc. 57 (2) (2011) 163–176, https://doi.org/10.1016/j.vibspec.2011.08.003.
[15] R.J. Dijkstra, C.T. Martha, F. Ariese, U.A.T. Brinkman, C. Gooijer, On-line identification method in column liquid chromatography: UV resonance Raman spectroscopy, Anal. Chem. 73 (20) (2001) 4977–4982, https://doi.org/10.1021/ac0103569.
[16] S.A. Asher, C.R. Johnson, Raman spectroscopy of a coal liquid shows that fluorescence interference is minimized with ultraviolet excitation, Science 225 (4659) (1984) 311–313, https://doi.org/10.1126/science.6740313.
[17] S.A. Asher, UV Resonance Raman spectroscopy for analytical, physical, and biophysical chemistry. Part 2, Anal. Chem. 65 (4) (1993) 201A–210A, https://doi.org/10.1021/ac00052a001.
[18] J. Neugebauer, E.J. Baerends, E.V. Efremov, F. Ariese, C. Gooijer, Combined theoretical and experimental deep-UV resonance Raman studies of substituted pyrenes, Chem. A Eur. J. 109 (10) (2005) 2100–2106, https://doi.org/10.1021/jp045360d.
[19] C.R. Johnson, S.A. Asher, A new selective technique for characterization of polycyclic aromatic hydrocarbons in complex samples: UV resonance Raman spectrometry of coal liquids, Anal. Chem. 56 (12) (1984) 2258–2261, https://doi.org/10.1021/ac00276a065.
[20] R. Altkorn, I. Koev, R.P. Van Duyne, M. Litorja, Low-loss liquid-core optical fiber for low-refractive-index liquids: fabrication, characterization, and application in Raman spectroscopy, Appl. Optics 36 (34) (1997) 8992–8998, https://doi.org/10.1364/AO.36.008992.
[21] B.J. Marquardt, P.G. Vahey, R.E. Synovec, L.W. Burgess, A Raman waveguide detector for liquid chromatography, Anal. Chem. 71 (21) (1999) 4808–4814, https://doi.org/10.1021/ac9907336.
[22] R.J. Dijkstra, C.J. Slooten, A. Stortelder, et al., Liquid-core waveguide technology for coupling column liquid chromatography and Raman spectroscopy, J. Chromatogr. A 918 (1) (2001) 25–36, https://doi.org/10.1016/S0021-9673(01)00721-X.
[23] J. Thissen, M.D. Klassen, M.C. Hacker, J. Breitkreutz, T. Teutenberg, B. Fischer, Online coupling of size exclusion chromatography to capillary-enhanced Raman spectroscopy for the identification of protein classes in hemolyzed blood serum, Anal. Bioanal. Chem. 417 (2) (2025) 335–344, https://doi.org/10.1007/s00216-024-05649-3.
[24] J. Thissen, M.D. Klassen, P. Constantinidis, et al., Online coupling of size exclusion chromatography to capillary enhanced Raman spectroscopy for the analysis of proteins and biopharmaceutical drug products, Anal. Chem. 95 (48) (2023) 17868–17877, https://doi.org/10.1021/acs.analchem.3c03991.
[25] T. Frosch, D. Yan, J. Popp, Ultrasensitive Fiber enhanced UV resonance Raman sensing of drugs, Anal. Chem. 85 (13) (2013) 6264–6271, https://doi.org/10.1021/ac400365f.
[26] D. Kottke, B.B. Burckhardt, J. Breitkreutz, B. Fischer, Application and validation of a coaxial liquid core waveguide fluorescence detector for the permeation analysis of desmopressin acetate, Talanta (2021) 122145, https://doi.org/10.1016/j.talanta.2021.122145.
[27] N.K. Vuchkov, K.A. Temelkov, P.V. Zahariev, N.V. Sabotinov, Influence of the active zone diameter, on the UV-ion ne-CuBr laser performance, IEEE J. Quantum Electron. 37 (12) (2001) 1538–1546, https://doi.org/10.1109/3.970900.
[28] S. Srinivasan, V. Renganayaki, Computational studies of vibration spectra and thermodynamic properties of metformin using HF, DFT methods, Mater. Sci. Res. India 8 (1) (2015) 165–172, https://doi.org/10.13005/msri/080124.
[29] A. Kramida, G. Nave, J. Reader, The Cu II Spectrum, Atoms 5 (1) (2017) 9, https://doi.org/10.3390/atoms5010009.

[30] K. Balci, The effects of conformation and intermolecular hydrogen bonding on the structural and vibrational spectral data of naproxen molecule, Vib. Spectrosc. 70 (2014) 168–186, https://doi.org/10.1016/j.vibspec.2013.12.002.
[31] T.G. Spiro, Resonance Raman spectroscopy. New structure probe for biological chromophores, Acc. Chem. Res. 7 (10) (1974) 339–344, https://doi.org/10.1021/ar50082a004.
[32] M.D. Morris, D.J. Wallan, Resonance Raman spectroscopy. Current applications and prospects, Anal. Chem. 51 (2) (1979) 182A–192A., https://doi.org/10.1021/ac50038a001.